Antioxidant Properties of Cerium Oxide Nanocrystals as a Function of Nanocrystal Diameter and Surface Coating

Seung Soo Lee,[†] Wensi Song,[‡] Minjung Cho,[†] Hema L. Puppala,[†] Phuc Nguyen,[†] Huiguang Zhu,[†] Laura Segatori,[‡] and Vicki L. Colvin[†,‡,*]

[†]Department of Chemistry, Rice University, Houston, Texas 77005, United States and [‡]Department of Chemical and Biomolecular Engineering, Rice University, Houston, Texas 77005, United States

ABSTRACT

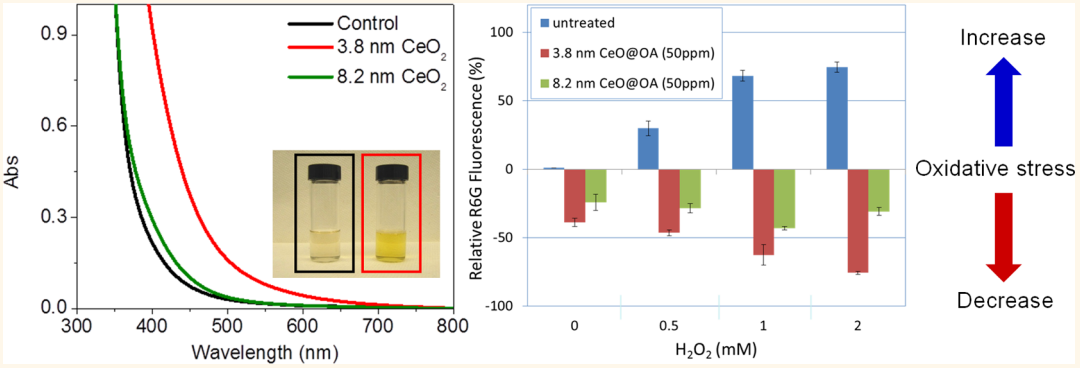

This work examines the effect of nanocrystal diameter and surface coating on the reactivity of cerium oxide nanocrystals with H_2O_2 both in chemical solutions and in cells. Monodisperse nanocrystals were formed in organic solvents from the decomposition of cerium precursors, and subsequently phase transferred into water using amphiphiles as nanoparticle coatings. Quantitative analysis of the antioxidant capacity of CeO_{2-x} using gas chromatography and a luminol test revealed that 2 mol of H_2O_2 reacted with every mole of cerium(III), suggesting that the reaction proceeds *via* a Fenton-type mechanism. Smaller diameter nanocrystals containing more cerium(III) were found to be more reactive toward H_2O_2. Additionally, the presence of a surface coating did not preclude the reaction between the nanocrystal surface cerium(III) and hydrogen peroxide. Taken together, the most reactive nanoparticles were the smallest (*e.g.*, 3.8 nm diameter) with the thinnest surface coating (*e.g.*, oleic acid). Moreover, a benchmark test of their antioxidant capacity revealed these materials were 9 times more reactive than commercial antioxidants such as Trolox. A unique feature of these antioxidant nanocrystals is that they can be applied multiple times: over weeks, cerium(IV) rich particles slowly return to their starting cerium(III) content. In nearly all cases, the particles remain colloidally stable (*e.g.*, nonaggregated) and could be applied multiple times as antioxidants. These chemical properties were also observed in cell culture, where the materials were able to reduce oxidative stress in human dermal fibroblasts exposed to H_2O_2 with efficiency comparable to their solution phase reactivity. These data suggest that organic coatings on cerium oxide nanocrystals do not limit the antioxidant behavior of the nanocrystals, and that their redox cycling behavior can be preserved even when stabilized.

KEYWORDS: cerium oxide · nanocrystal · Fenton-type reaction · redox cycle · antioxidant capacity

Cerium oxide (CeO_2, ceria) is a lanthanide metal oxide that by virtue of the redox potentials of cerium(III) and cerium(IV) can exhibit facile cycling between these two oxidation states.[1−4] As a result, ceria easily forms nonstoichiometric compositions, CeO_{2-x}, as cerium(IV) is reduced to cerium(III) leaving oxygen vacancies in the lattice.[5,6] In nanocrystals, these oxygen vacancies are thought to be clustered and stabilized at the particle surface which makes nanoscale ceria more effective at generating cerium(III) than the equivalent bulk material.[7,8] Cerium can also undergo redox cycling behavior as cerium(IV) is metastable in water and reverts to cerium(III)

* Address correspondence to colvin@rice.edu.

Received for review May 27, 2013 and accepted September 30, 2013.

Published online September 30, 2013
10.1021/nn4026806

under ambient conditions. This "oxygen buffering" behavior makes ceria ideal for applications such as water-gas shift catalysis, combustion catalysis, oxygen ion conductors, and solid oxide fuel cells.[7,9−21] More recently, the ability of cerium oxide nanocrystals to react with hydrogen peroxide in water has been demonstrated as a strategy for reducing unwanted reactive oxygen species (ROS) in biological systems.[22]

The precise mechanism governing cerium's reactivity toward hydrogen peroxide has been the subject of speculation. It was initially proposed that cerium(III) could react with H_2O_2 at the particle surface through direct reduction and oxidation.[23,24] More recently, Heckert *et al.* hypothesized that the reaction proceeds through an analog of the Fenton/Harbor-Weiss reaction[25] and H_2O_2 disproportionates into H_2O and O_2 at the cerium oxide surface.[22,25−27] Xue *et al.* showed that the hydroxyl radical (·OH) is produced during the reactions, an observation consistent with a Fenton reaction generated by H_2O_2.[28] Further confirmation of the chemical process behind nanocrystalline ceria's antioxidant properties has been limited as the reaction is typically characterized only through ultraviolet−visible absorption spectroscopy. In this approach, the reaction is tracked by monitoring the increase in Ce(IV), which presents a distinctive yellow color. Such data offer no quantitative information about the corresponding pace of hydrogen peroxide degradation.[24]

Over the past few years there has been increasing interest in the therapeutic capacity of nanoscale cerium oxide for diseases such as cancer, Alzheimer's, cardiac arrest, radiation induced cell death, and aging.[29−35] Das *et al.* reported that nanoceria protected adult rat spinal cord neurons against oxidative stress.[26] Perez *et al.* showed that the antioxidant properties of nanocrystalline ceria could improve cancer therapeutics: the pH-dependent antioxidant properties of nanocrystalline cerium oxide effectively provide normal cells, but not cancer cells, cytoprotection from oxygen radicals.[24] More recently, Kim *et al.* showed that cerium oxide nanocrystals reduced ischemic brain damage induced by reactive oxygen species in animals (Sprague−Dawley rats).[36] In summary, understanding the molecular mechanism that mediates the ability of nanocrystalline ceria to recycle back to their reactive state is crucial for designing the most effective nanocrystalline ceria for biomedical applications.[24,26]

It is unclear how the antioxidant capacity of nanoceria quantitatively compares to radioprotectants and antioxidants currently approved for clinical use.[26,29,35,37−50] The standard method to quantify antioxidant properties, the oxygen-radical absorbance capacity (ORAC) assay, is based on measuring a fluorescent indicator (β-phycoerythrin) in the presence of a radical initiator (2,2′-azobis(2-amidinopropane)dihydrochloride (AAPH)) and the target compound.[51] Target compounds with high antioxidant capacity react with ROS generated by the initiator, thereby preserving the intensity of the fluorescent indicator. Such assays are suitable for the analysis of nanoscale materials. Lucente-Schultz *et al.* showed that the antioxidant property of pegylated single-walled carbon nanotubes was about 5 times higher than that of a known standard, Trolox.[52] Additionally, *in vitro* assays are available to quantitatively measure the antioxidant properties of nanomaterials.[24] For instance, silver nanoparticles were shown to scavenge the ROS in cell culture and inhibit the reaction between fluorescein dyes and ROS.[53,54]

While the *in vitro* and *in vivo* antioxidative properties of nanoscale ceria are promising, the design rules for developing materials with optimal antioxidative properties are not yet defined. One limitation has been the challenge of obtaining quantitative measurements of antioxidant properties.[43] Moreover, the role of the particle coating in mediating the reaction between ROS and the nanocrystal surface seems important, but not fully characterized. On one hand, the coating on a nanocrystal must be thin enough to allow for facile surface reactions, yet highly stable so as to resist degradation caused by the reaction with ROS. This latter point is particularly important as surface coating degradation can yield particle aggregation, which would compromise a number of biological applications.

In this research, we synthesized libraries of monodisperse cerium oxide nanocrystals using the high temperature decomposition of cerium precursors; the resulting uniform particles were phase transferred to water with high efficiency (>80%) using poly(acrylic acid)−octylamine (PAAOA), oleic acid, polyethylene imine (PEI), and polymaleicanhydride-alt-1-octadecene (PMAO). After exposure to hydrogen peroxide, smaller particles outperformed larger particles in terms of net amount of reactivity by virtue of their higher cerium(III) concentrations. The mechanism of the reaction was investigated using both GC-MS to monitor byproducts and a Luminol test to quantify peroxide concentration. Results of these analyses indicated 2 mol of peroxide react with 1 mol of cerium(III), a finding that is consistent with a Fenton-like reaction. The antioxidant capacity of the best oleic acid/CeO_2 materials as measured using the ORAC assay was 9-fold higher than that of the standardly used antioxidant, Trolox. These effects were also seen in cell culture, where cerium oxide nanocrystals were able to protect fibroblasts against oxidative stress induced by exposure to hydrogen peroxide. Finally, over repeated cycles, the oleic acid coated CeO_2 was found to be the most effective material; for 18 cycles, one mole of cerium(III) could react with more than twenty moles of H_2O_2.

RESULTS AND DISCUSSION

Physico-Chemical Properties and Mechanism of Ceria Reactions with Hydrogen Peroxides. Near-spherical ceria nanocrystals with diameters ranging from 4 to 8 nm were prepared

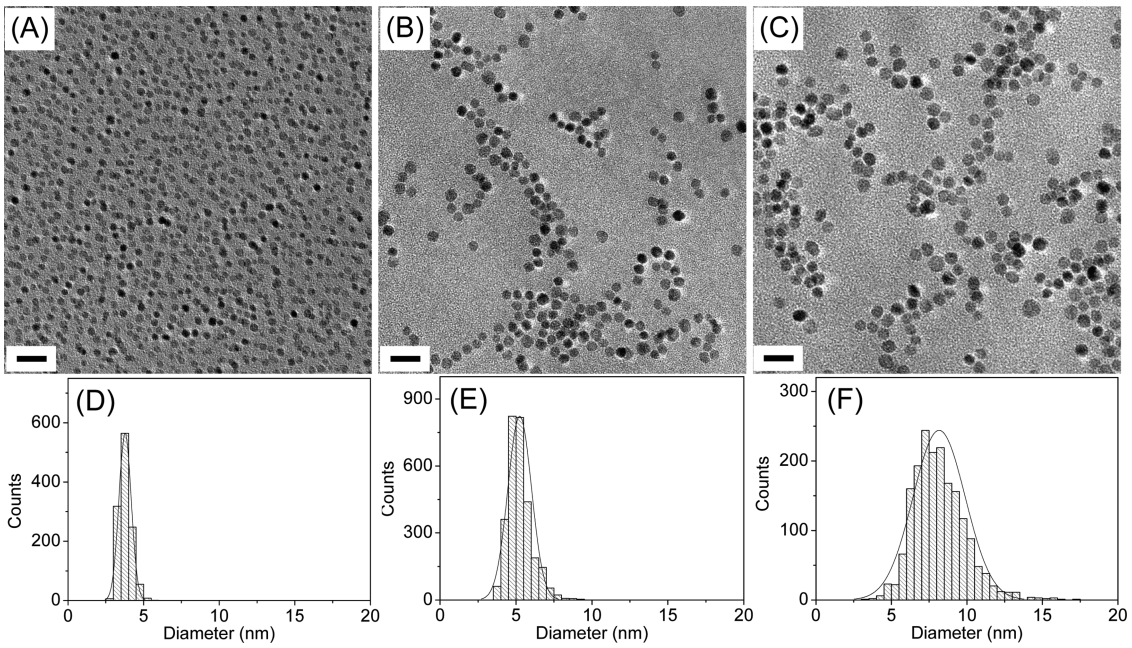

Figure 1. TEM micrographs (A–C) of water-soluble nanoceria. All scale bars are 20 nm from (A) to (C). (A) Oleic acid coated CeO_2 nanoparticles (3.8 ± 0.4 nm); (B) PEI coated CeO_2 nanoparticles (5.4 ± 1.0 nm); (C) PAAOA coated CeO_2 nanoparticles (8.2 ± 1.7 nm). The size distribution histograms (D–F) are placed at the bottom of the corresponding images. To analyze the size, over 1000 particles were measured in multiple images using the software package ImagePro.

by thermally decomposing cerium precursors in the presence of alkyl amines and water in 1-octadecene.[55] Figure 1 shows three different diameters of water-soluble nanocrystalline ceria produced from this reaction. The decomposition of cerium nitrate and oleylamine at 260 °C yielded the smallest nanocrystalline ceria. The addition of water promotes nanocrystal growth yielding nanocrystals up to 8 nm in diameter (8.2 ± 1.7 nm). Cerium oxide nanocrystals were phase transferred into aqueous solutions using amphiphilic surface agents such as fatty acids, copolymers, and polyethyleneimine.[55−58] The average diameters and morphology of the phase-transferred nanocrystals were identical to those observed for the as-prepared nanocrystals in organic solvents. Phase transfer yields exceeded 80% under the appropriate conditions (Figure S1).

The hydrodynamic diameters of the nanocrystalline ceria in water reflected the contributions from the inorganic core as well as the surface coating. The hydrodynamic diameters (D_H) of the four polymer coated cerium oxide nanocrystals are shown in Figure 2; these DLS measurements reveal that oleic acid and poly(acrylic acid)-octylamine (PAAOA) applied to nanocrystal cores of 3.8 nm diameter produced materials with hydrodynamic diameters (D_H) of 8.8 ± 1.8 and 6.8 ± 0.9 nm, respectively. PEI and PMAO are larger molecular weight polymers and these coatings yielded particles with D_H of 20.6 ± 2.2, and 17.9 ± 0.5 nm, respectively. The inset images (2 left-most panels) in Figure 2 illustrate the compact structures of the two thinnest coatings. The polymer coatings increased the hydrodynamic diameter irrespective of the core size of the nanocrystalline ceria. The zeta potential of oleic acid, PAAOA, and PMAO coated ceria nanocrystals were −52.1 ± 4.1, −41.4 ± 4.9, and −34.2 ± 1.8 mV, in contrast to amine functionalized polymer (PEI) coated ceria which was positively charged (43.5 ± 1.5 mV).

Most studies of the antioxidant properties of nanoscale ceria have used colorimetric methods to examine the progress of a particle's reaction with H_2O_2; colorless pale yellow cerium(III) gradually changes to the orange cerium(IV). Figure 3 shows how the absorption spectrum of a nanoceria suspension changes after H_2O_2 injection; the red-shift reflects the change of cerium(III) to cerium(IV).[59] The chemical reaction proposed to account for this color change is seen in Scheme 1.[39,60]

We verified that the shift in the absorption spectrum was consistent with changes in the cerium oxidation state using X-ray photoelectron spectroscopy (XPS). For example, after adding an excess of H_2O_2 to 3.8 nm cerium oxide, the cerium(III) concentration was reduced to 20% from nearly 50% prior to treatment (Figure S2). This finding illustrates that the active site on the surface of CeO_2 reacting with H_2O_2 is cerium(III) and that the capacity of a ceria nanocrystal to react with H_2O_2 will be sensitive function of the starting cerium(III) concentration.[61]

The underlying mechanism for the reaction between nanocrystalline ceria and hydrogen peroxide has been poorly defined for some time. While some investigators have proposed a direct reduction and oxidation process, others suggest the reaction has more in common with a Fenton-type process of the

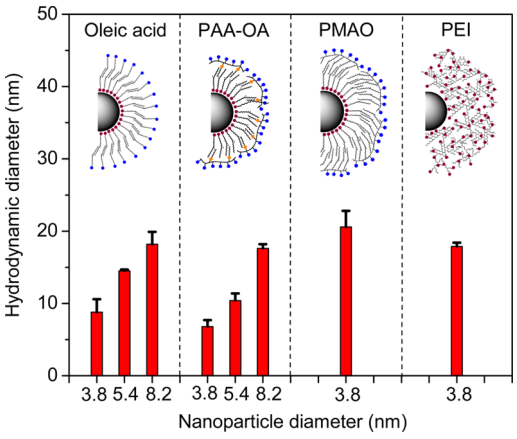

Figure 2. Hydrodynamic size of nanoceria. The cartoon images show oleic acid, PAAOA, PMAO, and PEI coated nanoceria. Carboxyl group, amide bond, and amine group, are represented using blue, yellow, and purple dots, respectively. The average diameters of nanoceria covered with oleic acid, PAAOA, PMAO, and PEI were analyzed by dynamic light scattering (DLS). All samples were measured in triplicates.

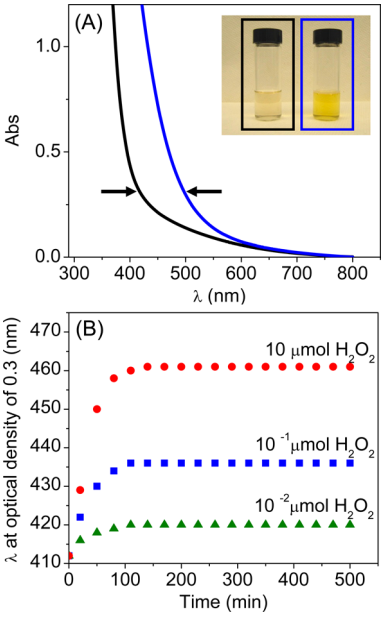

Figure 3. H_2O_2 quenching of water-soluble nanocrystalline cerium oxides. (A) The inset UV−vis band and the photo image demonstrate the red-shift from the control (black) to the as-reacted solution (blue) by the H_2O_2 injection. The 3.8 nm oleic acid coated nanoceria was used and the magnitude of the red-shifted wavelength of the UV−vis band ($\Delta\lambda$) was measured between the control and the red-shifted band at optical density of 0.3. (B) The increasing extent of the red-shift of nanoceria suspension (2.78 μM) depending on the higher concentrations of H_2O_2 from 10^{-2} to 10 μmol.

type illustrated in reaction mechanism above. Karakoti *et al.* hypothesized that the redox cycling of cerium ions occurs through Fenton type reaction producing hydroxyl anions and cerium peroxo complex. The formation of cerium−hydroxo or peroxo complexes may decrease the regeneration rate of Ce^{3+} when pH is

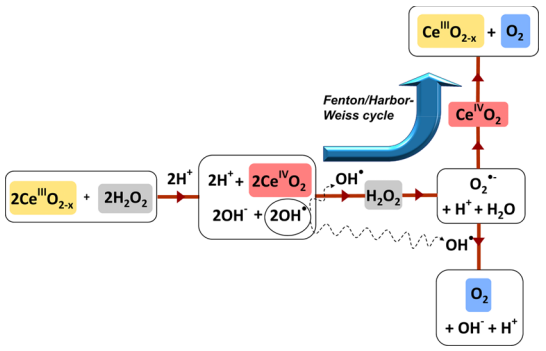

Scheme 1. Redox cycling of cerium oxide through Fenton-type reaction. Ce (III) reduces hydrogen peroxide and forms hydroxyl radicals and anions. These intermediate reactive oxygen species keep reacting with H_2O_2 and finally oxidized Ce (IV) is reduced to Ce (III) evolving oxygen (Fenton/Harbor-Weiss reaction; Ce(III):H_2O_2:O_2 is 1:2:1.) However, if the reduction of Cerium ion does not occur and hydroxyl radical reacts with super oxide anion, Ce (IV) is not reduced and the reaction ratio of cerium(III):H_2O_2:O_2 is 2:3:1.

more than 4.[22−25,28,39,60,62,63] These two mechanisms can be distinguished by the very different reactant molar ratios expected: a 2:1 reactivity between H_2O_2 and cerium(III) is anticipated for a Fenton-type process as opposed to a 1:1 or 1:2 relationships for direct redox reactions. Also relevant is the fact that Fenton reactions usually proceed through hydroxyl radical intermediates, and thus are more pronounced at lower pH values (Figure S3).[22,25]

To experimentally determine which mechanism may dominate for these particles, we measured the molar relationship between H_2O_2 and cerium(III) in this reaction. GC-MS was used to quantify the O_2 evolved by the disproportionation of H_2O_2 as a function of time after the injection of peroxide in a nanoceria solution.[64] In addition, the remaining (unreacted) H_2O_2 concentrations in nanoceria suspensions were measured by the luminol test.[65,66] To find the cerium(III) concentration, we used the nanocrystal total cerium concentration as determined from ICP-AES and the ratio between cerium(III) and cerium(IV) calculated from XPS (Figure S4).

These data, along with the pH dependence of the process, suggests that the antioxidant properties of nanocrystal ceria proceed through a Fenton type process. The amount of evolved oxygen after the decomposition of H_2O_2 by redox cycling of nanoceria was found by measuring the relative abundance ratio of oxygen to nitrogen in a sealed vial (see Methods and Figure S5).[67] The increasing O_2 evolution was monitored as a function of time. When the cerium(III) concentration was about 1 μmol (0.992 μmol), 1 and 2 μmol of H_2O_2 were fully decomposed by evolving about 0.5 and 1 μmol of O_2, respectively, whereas 5 and 10 μmol H_2O_2 addition left increasingly higher amount of unreacted H_2O_2 (Figure 4). The same molar ratio was also found independently be measuring the amount of

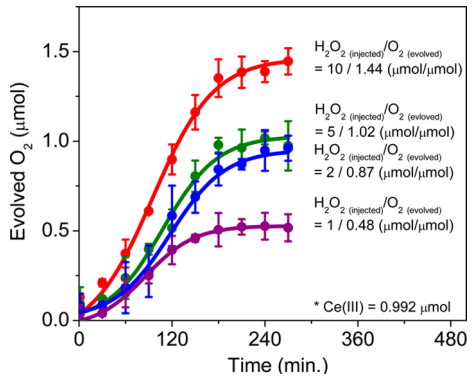

Figure 4. Quantitative analysis of H_2O_2 quenching of cerium oxide nanocrystals. The evolved oxygen concentration increased when H_2O_2 was decomposed in 2.78 μM nanoceria suspension (pH = 7, cerium(III) = 0.992 μmol). The concentration of evolved oxygen was monitored and measured by GC-MS as a function of time. The ratio of H_2O_2 to cerium(III) was 2 to 1 (H_2O_2 decomposition reaction; $2H_2O_2 \rightarrow 2H_2O + O_2$). The measurements were repeated three times.

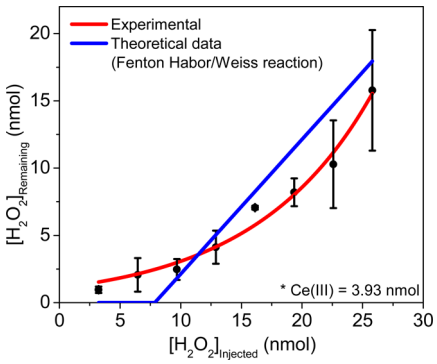

Figure 5. Quantitative analysis of H_2O_2 quenching of cerium oxide nanocrystals. The remaining (unreacted) H_2O_2 in a supernatant of nanoceria solution was measured by chemiluminescence from the reaction with luminol and peroxide after the separation of nanoceria using the ultracentrifugation method. The 3.8 nm oleic acid coated cerium oxide was utilized with the increase in the injections of H_2O_2. On the basis of the calibration curve (Figure S7), the remaining molar H_2O_2 was obtained from the equation: $y = 9.0 \times 10^6 x$ (y = the intensity of luminescence, x = mole of H_2O_2). The theoretical data of the remaining H_2O_2 was obtained by the equation: $[H_2O_2]_{remained} = [H_2O_2]_{injected} - 2 \times 3.93$ (nmol of cerium(III)) in the solution; 1 mol cerium(III) decomposes 2 mol H_2O_2 in the Fenton-like reaction.

unreacted peroxide using a Luminol test (see Supplemental discussions and Figures S4 and S6). Figure 5 shows that the experimental curve obtained from the amount of unreacted peroxide fit well to the expectation of a Fenton-like reaction (the ratio between cerium ion and H_2O_2 is 1 to 2).[25] Moreover, we can correlate the shift in the absorption spectrum to the generation of oxygen through this process. As Ce(III) is converted to Ce(IV), the color of the solution changes roughly linearly with the amount of Ce(III) converted; Figure S7 shows that as more of this is converted, you get more oxygen with a 0.0298 slope (evolved O_2 per UV−vis band shift, μmol/nm). Finally, consistent with this data is the observation that the reaction is pH dependent. Specifically at lower pH values it is more reactive (Figure S3).

Benchmarking Antioxidant Capacity and Trends with Size and Surface Coating. A critical question to address is what the capacity is for different particles, with different sizes and coatings, to react with hydrogen peroxide through the Fenton-type chemistry described above. For the purposes of this discussion, we refer to this parameter as the antioxidant capacity so as to align our discussion with the literature on antioxidants.[25,51,65] One convenient way to characterize the antioxidant capacity and compare it across samples is to use colorimetric data to indicate the amount of Ce(IV) produced. Here we defined the shift ($\Delta\lambda$) by measuring the wavelength of 0.3 optical density before and after peroxide addition. For example, 100 nmol of H_2O_2 led to only a 10 nm red shift, while 10 μmol of H_2O_2 led to a shift of 50 nm absorbance wavelength. This data shows that adding more peroxide increases the shift of the spectrum as more Ce(IV) is produced. However, for all samples there is a saturation point at which further addition of peroxide leads to no change. For example, for the former samples the absorption shift remained the same between 10 and 15 μmol of H_2O_2 addition. For these measurements, all nanoparticle solutions were fixed at 2.78 μM of ceria concentration (cerium(III) concentrations on the surfaces of the nanoparticles are 1 μmol; see Supplemental discussion). Note that the molecular weight of the nanoparticles varies sensitively with their diameter, but for a 3.8 nm nanocrystal, the equivalent particle concentration is roughly 10 pM.

These colorimetric tests reveal that the smallest nanoceria has the largest absorption change after the addition of H_2O_2 and hence greatest antioxidant capacity (Figure 6). We attribute this to both the higher concentration of cerium(III) in these nanocrystals and the increased stability of the cerium(IV). The smallest particle has the greatest concentration of cerium(III) on the surface of nanoceria because of the increasing lattice expansion and the release of oxygen atoms.[7,8,68] For example, we found that the cerium(III) concentrations from different diameter ceria samples were 44, 39 and 30% from 3.8, 5.4, and 8.2 nm cerium oxide, respectively.[55] All of the various surface coatings showed similar trends: smaller nanocrystals had higher antioxidant capacities. For example, PAAOA coated 3.8 nm CeO_2 after treatment with excess H_2O_2 had $\Delta\lambda$ of 215 as compared to 8.2 nm diameter nanoceria having only $\Delta\lambda$ of 37 nm.

In addition to the diameter of the nanocrystalline ceria, the surface coating also played a significant role in defining the reactivity of the material. Specifically, when nanocrystals were coated with thicker polymers their antioxidant capacity diminished. Figure 6 shows the shift in the extent of H_2O_2 quenching capacity for four different polymer coating materials (oleic acid, PAAOA, PEI, and PMAO) for 3.8 nm diameter ceria

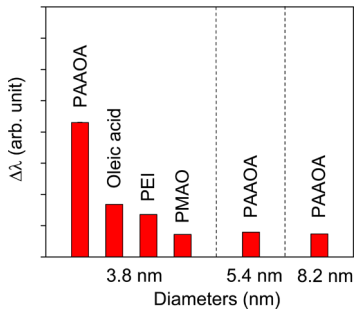

Figure 6. The different extents of H_2O_2 quenching capacity depending on various diameters and surface stabilizers on nanoceria. To compare the surface polymer dependent H_2O_2 quenching efficiency of nanoceria, the extent of the band shift ($\Delta\lambda$) was measured at 0.30 absorbance after the injection of H_2O_2 from the control. For the diameter dependent H_2O_2 quenching, three different diameter CeO_2 suspensions were utilized (d = 3.8, 5.4, 8.2 nm; PAAOA coated CeO_2). Surface coating dependent H_2O_2 quenching was shown by 3.8 nm CeO_2 covered with four different polymers (PAAOA, oleic acid, PEI, and PMAO).

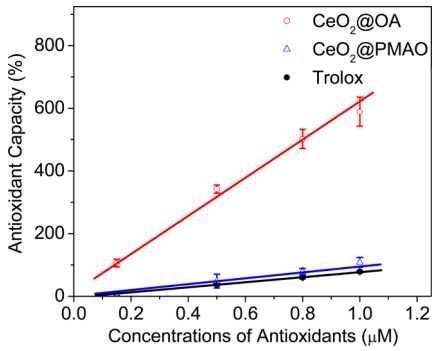

Figure 7. Antioxidant capacity of cerium oxide nanocrystals. The capacity was calculated from the equation mentioned from Lucio *et al.*[69] The slopes of the trend lines from oleic acid coated (red), PMAO coated (blue), nanoceria and Trolox (black) are 616.02, 95.76, and 73.24, respectively. All measurements were repeated three times.

cores. PAAOA coated nanoceria, as expected, had the largest red-shift corresponding to the most reactivity toward hydrogen peroxide. The reactivity of other polymer coatings scaled well with their thickness as measured using dynamic light scattering (Figure 2). We speculate that the very thinnest surface coatings present small kinetic barriers to the interfacial reaction between H_2O_2 and cerium(III), while thicker polymer molecules block surfaces from H_2O_2. While we generally gave the system enough time to react so our observations would reflect equilibrium, we did observe that the thinnest surface coating (*e.g.*, oleic acid on CeO_2) became saturated within only 30 min as compared to the thicker polymer coated ceria (*e.g.*, PMAO coated CeO_2) which required 90 min (Figure S8).

Absorption spectroscopy is an excellent method to compare relative quenching capacities among particles, but these data do not provide a benchmark against known antioxidant and radiation protection molecules already widely used. For this purpose, we applied a standard test, the ORAC assay,[52] to the best performing nanocrystalline ceria from the peroxide tests: nanocrystalline ceria with 3.8 nm core diameter coated with oleic acid. This test monitors how the fluorescence from a Fluorescein salt persists in the presence of an antioxidant which scavenges ROS generated by the radical initiator, AAPH. A fluorescence intensity that persists for a long time indicates a strong antioxidant.

This ORAC assay revealed that the antioxidant capacity of oleic acid coated cerium oxide was 9 times higher than that of a water-soluble derivative of Vitamin E, Trolox (Figure 7). In this assay, all antioxidant samples (nanoceria and Trolox) were stored in PBS (pH = 7) from 0.1 to 1 μM and the fluorescence intensity was monitored every minute for 6 h after the injection of 45 mM of AAPH as shown in Figure S9. The thinnest surface coating (oleic acid) present on cerium oxide nanocrystal allows more radical scavenging than the thickest polymer (PMAO) on the nanocrystal; to put things in perspective, PMAO coated cerium oxide nanocrystal has an antioxidant capacity comparable to Trolox. Furthermore, cerium oxide nanocrystal showed efficacy at submicromolar concentrations in cerium oxide, and even nanomolar concentrations with regards to the entire particles. In comparison, standard concentrations of 1−10 μM vitamin E or single-walled carbon nanotubes are typically applied.[51,52,69] We also note that oleic acid coated ceria is nontoxic at these concentrations in an MTS assay using HDF cell line; LD_{50} is 1.8 μM as shown in Figure S10. These data suggest that the oleic acid coated nanoceria could be a potent antioxidant material with high radical scavenger capacity and low toxicity.

To understand how the observed antioxidant properties of cerium oxide nanocrystal affect biological system, we investigated the ability of nanocrystalline ceria to protect cells from oxidative stress induced by hydrogen peroxide exposure. We measured the generation of intracellular reactive oxygen species (ROS) in fibroblasts pretreated with cerium oxide nanocrystals and exposed to hydrogen peroxide. To explore the antioxidant capacity of cerium oxide nanocrystals toward H_2O_2-induced oxidative stress in fibroblasts, cells were cultured in the presence of cerium oxide nanocrystals at 37 °C for 1 day. Relatively low nanocrystal exposures (50 ppm of cerium) were employed, which resulted in over 90% viability as observed using the MTS assay during the first exposure (the LD_{50} value for 3.8 nm was 94.9 ppm (1789.9 nM of nanocrystals); and for 8.2 nm cerium oxide nanocrystals, 87.7 ppm (87.2 nM of nanocrystals)). Concentrations higher than the LD_{50} resulted in cell death. The cells were then washed, and the medium was replaced with fresh medium containing a large dose of H_2O_2 (2 mM). In this experimental scheme, only ceria nanocrystals that were internalized could be responsible for any observed protective effect.

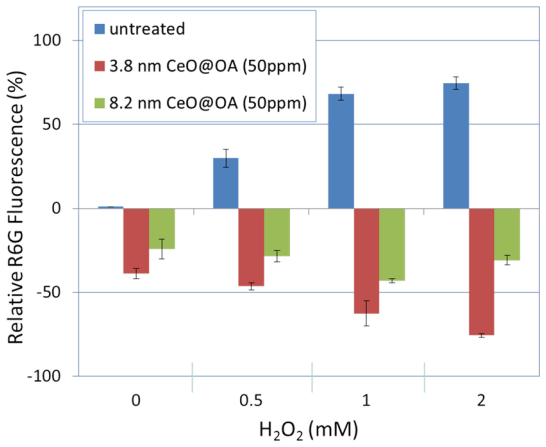

Figure 8. Cerium oxide prevents hydrogen peroxide-induced generation of intracellular ROS. ROS generation in fibroblasts untreated (blue), treated with 3.8 nm cerium oxide (red), or treated with 8.2 nm cerium oxide (green) for 24 h and subsequently exposed to hydrogen peroxide was quantified by measuring R6G fluorescence (%) as described in the Methods section.

To investigate whether cerium oxide nanocrystals protects cells from oxidative stress we quantified the generation of ROS in fibroblasts exposed to hydrogen peroxide upon treatment with cerium oxide nanocrystals. Oxidative stress was evaluated using dihydrorhodamine 6G, a cell permeable molecule that is oxidized to fluorescent rhodamine 6G (R6G) upon induction of oxidative stress.[53] Therefore, the fluorescence intensity of R6G is an indication of oxidative stress in cells. Cells pretreated with cerium oxide nanocrystals were exposed to a range of hydrogen peroxide concentrations, under conditions previously reported to cause oxidative stress.[70] As expected, R6G fluorescence was found to increase as a function of hydrogen peroxide concentration reaching 74% increase in cells exposed to 2 mM hydrogen peroxide compared to untreated cells (Figure 8). However, pretreatment with cerium oxide dramatically reduced generation of ROS, resulting in 75 and 30% decrease in R6G fluorescence in cells pretreated with 3.8 and 8.2 nm cerium oxides, respectively. Interestingly, the smaller cerium oxide nanocrystals (3.8 nm) displayed higher antioxidant properties than the larger cerium oxides nanocrystals (8.2 nm). We suggest that the highest percent of cerium(III) in the smaller nanocrystals (44% of Ce(III) from 3.8 nm cerium oxide) prevents accumulation of intracellular ROS more effectively than the larger cerium oxide nanocrystal (30% of Ce(III) from 8.2 nm cerium oxide). In summary, these results demonstrate that oleic acid coated cerium oxide nanocrystals protect cells from oxidative stress by preventing generation of intracellular ROS. It remains to be determined how size and other physicochemical properties of the cerium oxide nanocrystals affect cell physiology. The intracellular localization of the nanocrystals as well as cellular pathways activated in response to internalization of the nanocrystals will also need to be determined to define the design rules to generate the nanocrystals with desired antioxidative properties. (Figure S11)

Recycling Behavior of Nanoscale Ceria and Its Dependence on Surface Coating. One finding from this work is that nanoparticles may be reused as antioxidants because cerium(IV) can in some cases slowly recycle back to cerium(III). Das *et al.* demonstrated this feasibility of the redox cycling of cerium ions using nanoceria prepared by coprecipitation method; the pale yellow solution formed after hydrogen peroxide reaction passively returned to its original position in a matter of days (Figures S12 and S13).[26] As is apparent, many of these samples can be used repeatedly, presumably after native donors present in water have converted the cerium(IV) back to cerium(III).

However, after multiple uses, nanoparticles can either exhibit reduced reactivity toward hydrogen peroxide, or they can precipitate out of solution. In the data in Figure S12 this is shown with an arrow, after which no meaningful data could be collected. This phenomenon is analogous to a catalyst poisoning process. If particles are to be optimized for long-term redox cycling stability, the factors that improve the ability to recycle the material must be identified. To compare across these materials, we calculated the total number of moles of peroxide per mole of cerium(III) (note: not per mole of nanocrystals) that react with the particles without resulting in precipitation.

From the perspective of multiple redox cycling, oleic acid coated nanoceria had the longest lifetime; oleic acid coated ceria did not lose its colloidal stability even after 18 injections of H_2O_2 over 6 months (10 μmol of H_2O_2 injection per cycle, 18 cycles) (Figure S12). This material can react with 20 times more peroxide than cerium(III) concentration for 18 cycles; CeO_2 suspension under the multiple H_2O_2 injections showed 21.6 μmol of H_2O_2 decomposition for 18 cycles based on the results from GC-MS and UV–vis in Figure S7. We speculate that oleic acid not only forms the hydrophilic second layer by hydrophobic–hydrophobic interaction with 18-carbon chain on oleylamine, but also makes the first layer more compact through stronger interaction between oleic acid and ceria.[56] Multiple injections of H_2O_2 gradually reduced the reactivity of the nanocrystals; after 18 cycles of the redox reaction, oleic acid coated nanoceria lost almost 90% of its reactivity as compared to the first hydrogen peroxide exposure. Eventually, we anticipate that the surface coating itself reacts with excess H_2O_2 and becomes less effective at stabilizing nanocrystals leading to aggregation and loss of antioxidant behavior.[71–73] (Figure S14)

CONCLUSIONS

Monodisperse cerium oxide nanocrystals were synthesized with uniform diameters by the high temperature decomposition of cerium precursors in organic

media. The resulting nanocrystals were phase transferred to water *via* a bilayer method using amphiphilic polymers (poly(acrylic acid), oleic acid, and polymaleicanhydride-alt-1-octadecene) as well as a ligand exchange route by the addition of polyethylene imine. During the reaction between these nanocrystals and peroxide, the evolved O_2 and the remaining H_2O_2 concentration were monitored using GC-MS and a luminol test; the ratio of the reacted H_2O_2/cerium(III)/O_2 was almost 2:1:1. These results illustrated that colloidally stable oleic acid coated cerium oxide quench H_2O_2 molecules through a Fenton-like reaction. The antioxidant capacity of ceria depends on cerium(III) concentration and the polymer shell thickness; 3.8 nm diameter cerium oxide nanocrystals (44% cerium(III) content) coated with a thin surface stabilizer (such as poly(acrylic acid) or oleic acid) quenched more H_2O_2 than 8.2 nm diameter nanoceria (30% cerium(III) content) covered with thicker polymer (polyethylene imine or polymaleicanhydride-alt-1-octadecene) stabilizers. The antioxidant capacity as evaluated using the ORAC assay of the thinnest surface coated nanoceria (3.8 nm CeO_2 coated with oleic acid) was 9-fold higher than that of a benchmark antioxidant, Trolox. Furthermore, these nanocrystals reduced intracellular ROS generation in fibroblasts exposed to oxidative stress. During repeated use of nanoscale CeO_2 over months, the oleic acid coatings retained their stability in the presence of H_2O_2. Ultimately the particles were able to react over 20 times with high concentrations of hydrogen peroxide. The relatively high antioxidant capacity of these materials, coupled with their ability to be reused, suggests that the need to incorporate surface coatings onto nanocrystalline ceria is not an impediment to their application to biological problems.

METHODS

Chemicals. Cerium(III) nitrate hexahydrate ($Ce(NO_3)_3\cdot 6H_2O$ (99%)),oleylamine (OM, technical grade, 70%), 1,2 hexadecanediol (HDD, technical grade, 90%), 1-octadecene (ODE, technical grade, 90%), poly(acrylic acid) (PAA, $M_w = 1800$), octylamine (99%), polymaleicanhydride-alt-1-octadecene (PMAO, M_w = 30 000−50 000), polyethyleneimine (PEI, M_w = 25 000), tris(hydroxyl methyl)-aminomethane (99.9%), luminol (97%), potassium ferricyanide ($K_3Fe(CN)_6$, 99%), fluorescein sodium salt (FL), 2-2′-azobis(2-amidinopropane)dihydrochloride (AAPH), and racemic 6-hydroxy-2,5,7,8-tetramethylchromane-2-carboxylic acid (Trolx) were purchased from Sigma-Aldrich. Hydrogen peroxide (H_2O_2, 30%), sodium hydroxide (NaOH, 1 N), sodium bicarbonate ($NaHCO_3$, 99.9%) and dimethylformamide (DMF, 99.9%) were purchased from Fisher scientific. 1-Ethyl-3-[3-dimethylaminopropyl]carbodiimide hydrochloride (EDC) was purchased from Thermo Scientific. All ceria nanocrystals were synthesized under ultrahigh purity nitrogen.

Synthesis of Nanoceria. Three different diameter cerium oxide nanocrystals were synthesized by the decomposition of $Ce(NO_3)_3\cdot 6H_2O$ in the presence of oleylamine at high temperature as reported previously by this group.[55] The 3.8 nm cerium oxide was synthesized by 1 mmol of $Ce(NO_3)_3\cdot 6H_2O$ mixed with 3 mmol of oleylamine in 5 g of ODE. The 5.4 nm nanoceria was prepared by mixing 5 mmol of $Ce(NO_3)_3\cdot 6H_2O$ and 15 mmol of oleylamine in 5 g of ODE. The 8.2 nm nanoceria was obtained by adding water of 40 mmol in the cerium precursor and oleylamine mixture: the concentration of $Ce(NO_3)_3\cdot 6H_2O$ and oleylamine was 10 and 40 mmol, respectively, in 5 g of ODE. All chemicals were mixed at room temperature and dissolved at 80 °C for 30 min. Nanocrystals were grown at 260 °C for 2 h under ultrahigh pure nitrogen condition.

The as-prepared nanoceria was purified using ethanol, acetone and hexane at least 5 times to remove unreacted cerium precursor, surfactants, and ODE. The resulting deep brown precipitate gave pure ceria nanocrystals which are redispersible in various nonpolar solvents such as, chloroform, hexane and toluene.

Phase Transfer of Nanoceria. The as-synthesized nanoceria was transferred to aqueous solution using ligand exchange[57] and encapsulation methods.[56,58,74]

Oleic Acid Coated Nanoceria. Particular amount of oleic acid (from 30 to 250 μmol) was stirred with 1 mL of nanoceria/ethyl ether solution (typically, 5.4 mg/mL) and 10 mL of ultra pure water. Aqueous and organic phases were mixed by application of a probe-sonicator (UP 50H, DR.HIELSCHER) for 5 min at 60% amplitude and full cycle. The resulting solution was further stirred for 1 day to evaporate the ether and to obtain a clear yellow brown solution.

Poly(acrylic acid)−Octylamine (PAAOA) Coated Nanoceria. The synthesis of PAAOA amphiphilic polymer was adapted from previous reports.[75,76] Various concentrations of PAAOA (from 0.5 to 50 μmol) were added to 1 mL of nanoceria/ethyl ether solution (typically, 2.5 mg/mL) with 10 mL of ultra pure water. The mixed solution was sonicated using the probe sonicator at the same experimental setup mentioned above.

PMAO Coated Nanoceria. PMAO (0.01−2.5 μmol) was added to 1 mL of nanoceria/chloroform solution (about 1 mg/mL) with 10 mL of ultra pure water. The solution was probe-sonicated in the same condition mentioned above.

PEI Coated Nanoceria. PEI (0.1−16 μmol) was added to 1 mL of nanoceria/chloroform solution (about 5.7 mg/mL) then probe-sonicated with the same condition, mentioned above.

Purification of as-prepared water-soluble nanoceria was carried out using ultracentrifugation (Sorvall Discovery 100 SE Ultracentrifuge) at 40 000 rpm for 4 h, followed by syringe filtration (pore size of 0.45 μm, WHATMAN-NYL). All the resulting phase transfer nanoceria pellets were redispersed and stable in Mili-Q water, phosphate or sodium bicarbonate buffer solution (pH was from 5 to 10).

UV−Vis Spectroscopy. To measure antioxidant property of different diameter and surface coated nanoceria with H_2O_2, UV−vis absorbance spectra were obtained as a function of time using UV−vis spectroscope (Cary 5000 UV−vis-NIR spectrophotometer, Varian).

Transmission Electron Microscopy (TEM). The TEM micrographs were taken by a JEOL 2100 field emission gun TEM operating at 200 kV with a single tilt holder using ultrathin carbon type-A 400 mesh copper grids (Ted Pella, Inc.). The size and its distribution data were obtained by counting >1000 nanocrystalline particles using Image-Pro Plus 5.0 (Media Cybernetics, Inc., Silver Spring, MD).

X-ray Photoelectron Spectroscope (XPS). XPS data was collected using a PHI Quantera XPS with a monochromatic Aluminum 38.6 W X-ray source and 200.0 μm X-ray spot size with a pass energy of 26.00 eV at 45.0°.

Dynamic Light Scattering (DLS) Analysis. The phase-transfer water-soluble nanocrystalline cerium oxide samples were characterized by dynamic light scattering (DLS) and zeta potential to measure the hydrodynamic size and surface charge, respectively. The hydrodynamic diameters and surface charge of different sized nanoceria covered with PAAOA, oleic acid, PMAO, and PEI were measured at pH 7 and 25 °C, using a Malvern Nano ZS system by Malvern Instruments equipped

with a HeNe 633 nm laser (Malvern Zetasizer Nanoseries, Malvern, U.K.). The average hydrodynamic diameters were obtained by the mean size of the first peak of the number distribution and the standard deviation was determined from triplicate measurements.

Inductively Coupled Plasma Atomic Emission Spectroscopy (ICP). The concentration of water transferred nanoceria was measured from ICP using a Perkin-Elmer ICP-AES instrument equipped with an auto sampler. ICP samples were prepared by digestion of aqueous fractions using HNO_3 (99%) and H_2O_2 (30%) in a 5 mL of diluted nanoceria sample. The solution volume was decreased by heating to a fourth of its original volume. When the solution was dried to about 1/4 of the initial volume, 100 μL nitric acid was added. The obtained sample was treated by the further addition of 50 μL of nitric acid and 1 mL of H_2O_2 until effervescence stopped, indicating full dissolution of the ceria. The resulting colorless solution was transferred into a 5 mL volumetric flask and then diluted to 5 mL using DI-water.

Nanoparticle Concentration Calculation. Nanoparticle concentrations are found from analytical measures of total cerium concentration in solutions digested with acids. To require an estimate of the weight of a single particle, we assumed a particle volume of $4/3\pi r^3$ where r is the average radius of the nanocrystal as determined by TEM measurements of over 1000 particles; then we took the density of CeO_2 in the nanoparticle to be equivalent to that of the bulk phase (*e.g.*, 7.65 g/mL) and could calculate the particle weight.[55] As an example, the volume of a 3.8 nm diameter particle of CeO_2 is 2.87×10^{-20} mL, which provides a total mass per particle of 2.2×10^{-19} g. Using this data, and Avogadro's number, we find for a solution 300 ppm in cerium a nanoparticle concentration of 2.78 μM.

GC-MS Spectroscopy. Agilent Technologies 7890A GC system was used to measure the evolved oxygen amount during the decomposition of H_2O_2 in nanoceria solution. For the calibration of O_2 measurement, the vials (National Scientific Company (vial, C4020-210; septa, C4020-36A)) were purged with nitrogen for 5 min, various amounts of oxygen (0, 500, 1000, and 1500 μL) were injected into N_2 purged vials, and 10 μL of the sample was injected into GC-MS using Pressure-Lok gas syringe (VICI Precision Analytical Syringe, Vacuum leak rate was less than 2.8×10^{-3} μL/h.). These measurements were conducted in triplicates. Concentration (ppm) was calculated by considering the purged vials to be at 1 atm, and then getting mass of the oxygen. The equation of oxygen calibration curve was $y = 0.0007x$; y is relative abundance ratio of oxygen to nitrogen (I_{O2}/I_{N2}) and x is oxygen content (ppm) (Figure S5).

To explore the abundance of evolved oxygen in nanoceria samples, the relative intensity ratios of oxygen to nitrogen were collected as a function of time after the injection of particular amount of H_2O_2 (1, 2, 5, and 10 μmol) in nanoceria solution (2.78 μM) in a 10 mL crimped vial.[67]

Luminol Test of Water-Soluble Cerium Oxide Nanocrystals. H_2O_2 (6.45×10^{-4} M) from 0 to 50 μL was injected to an oleic acid coated 3.8 nm cerium oxide solution (0.011 μM). To measure the remaining concentration of H_2O_2 in the supernatant, the reaction solution was centrifuged at 43 000 rpm for 7 h. To measure chemiluminescence, 20 μL of the supernatant was mixed with 120 μL of tris(hydroxyl methyl)-aminomethane buffer (pH ~ 10), 50 μL of 3% $K_3Fe(CN)_6$, and 10 μL of luminol (1×10^{-2} M, pH ~ 10) in a 96-well plate(flat bottom, white polystyrene). The absorbance was measured at 485 nm by a spectrophotometer (SpectraMax M2, Molecular Devices, Sunnyvale, CA). This experiment was repeated in triplicate.

Oxygen-Radical Absorbance Capacity (ORAC) Assay. The assay was treated by the method mentioned by Lucente-Schultz *et al.*[52] Fluorescein sodium salt (FL, 0.2 μM), 2-2′-azobis(2-amidinopropane)-dihydrochloride (AAPH, 0.15 M), and racemic 6-hydroxy-2,5,7,8-tetramethylchromane-2-carboxylic acid (Trolx, from 1.5 to 10 μM), and nanoceria (oleic acid coated- and PMAO coated-CeO_2, from 1.5 to 10 μM) were prepared in phosphate buffer saline (PBS) at pH 7.4 in a 96-well plate (flat bottom, black with clear bottom, polystyrene). The fluorescence intensity was measured at 530 nm by 485 nm excitation every minute for 6 h using a microplate reader (TECAN Infinite M200). The relative fluorescence intensity was measured by the assay (with antioxidant: 120 μL FL + 20 μL antioxidant + 60 μL AAPH), Control 1 (without AAPH: 120 μL FL + 20 μL antioxidant + 60 μL PBS), and Control 2 (without FL: 120 μL PBS + 20 μL antioxidant + 60 μL PBS). The antioxidant capacity was calculated by measuring the area under curve (AUC) of the time dependent fluorescence intensity from the antioxidant (Trolox and nanoceria) and the blank (without the antioxidant) reported by Lúcio *et al.*[69] The assays were performed in triplicates.

$$\text{Antioxidant capacity}(\%) = \frac{\text{AUC}_{\text{Antioxidant}} - \text{AUC}_{\text{Blank}}}{\text{AUC}_{\text{Blank}}} \times 100$$

Measurement of Intracellular Reactive Oxygen Species (ROS) Generation. Wild-type human dermal fibroblasts were obtained from Coriell Cell Repositories (GM00498). Fibroblasts were grown at 37 °C in 5% CO_2 in DMEM (Lonza), supplemented with 10% heat-inactivated fetal bovine serum and 1% glutamine Pen-Strep. Medium was replaced every 3 or 4 days. Monolayers were passaged with TrypLE Express. Oxidative stress was measured using Dihydrorohodamine 6G (DHR6G) as previously described by Kilpatrick *et al.*[77] Cells were cultured in medium containing cerium oxide nanocrystals for 24 h at 37 °C. The medium was replaced with fresh medium containing 2 mM hydrogen peroxide (H_2O_2) and samples were incubated for 2 h at 37 °C. Cells were washed with PBS and incubated with 5 μM DHR6G (Anaspec) in serum-free DMEM for 30 min at 37 °C. Cells were collected in PBS, centrifuged at 300*g* for 5 min, and washed with PBS. The fluorescence (FL) intensity was analyzed by flow cytometry (FACSCantoII, BD Biosciences) using a 488-nm argon laser and 585/42 band-pass filter. The relative fluorescence ($FL_{relative}$, %) was calculated as follows:

$$\text{FL}_{\text{Relative}}(\%) = \frac{\text{FL}_{\text{Treatedcells}} - \text{FL}_{\text{Untreatedcells}}}{\text{FL}_{\text{Untreatedcells}}} \times 100$$

Conflict of Interest: The authors declare no competing financial interest.

Acknowledgment. This work was supported by the Center for Biological and Environmental Nanotechnology (NSF grant EEC-0647452), Advanced Energy Consortium (UTA/AEC BEG08-011), and Welch foundation (C-1824). P.N. was funded from NSF REU Site (NSF award EEC-0852008).

Supporting Information Available: Phase transfer efficiency of ceria nanocrystals, XPS data of ceria before and after H_2O_2 injection, pH dependent antioxidant capacity, the calculations of cerium(III) on the surface of nanoceria, the calibration curve of O_2 in GC-MS analysis, the H_2O_2 calibration curve for the luminol test, the magnitude of the red shift UV−vis band of oleic acid and PMAO coated ceria nanocrystal suspension after H_2O_2 injection, loss of colloidal stability of PEI coated 3.8 nm nanoceria after H_2O_2 injection, TEM image of nanoceria after H_2O_2 injection, decomposed H_2O_2 calculation using the red shift UV−vis band and GC-MS data, antioxidant capacity of ceria nanocrystal suspension depending on different amount of H_2O_2 injections for 18 cycles, oxygen-radical absorbance capacity (ORAC) assay of nanoceria and Trolox, cell viability of Human Dermal Fibroblast (HDF) cell line in the presence of 3.8 nm oleic acid coated cerium oxide nanocrystals, bright field images of human dermal fibroblasts treated with cerium oxide nanocrystals, a table of XPS analysis of the individual peaks, and a table of the intracellular concentration of the nanocrystals. This material is available free of charge *via* the Internet at http://pubs.acs.org.

REFERENCES AND NOTES

1. Otsuka, K.; Wang, Y.; Sunada, E.; Yamanaka, I. Direct Partial Oxidation of Methane to Synthesis Gas by Cerium Oxide. *J. Catal.* **1998**, *175*, 152–160.
2. Otsuka, K.; Ushiyama, T.; Yamanaka, I. Partial Oxidation of Methane Using the Redox of Cerium Oxide. *Chem. Lett.* **1993**, 1517–1520.
3. Heckert, E. G.; Karakoti, A. S.; Seal, S.; Self, W. T. The Role of Cerium Redox State in the SOD Mimetic Activity of Nanoceria. *Biomaterials* **2008**, *29*, 2705–2709.

4. Liu, X. W.; Zhou, K. B.; Wang, L.; Wang, B. Y.; Li, Y. D. Oxygen Vacancy Clusters Promoting Reducibility and Activity of Ceria Nanorods. *J. Am. Chem. Soc.* **2009**, *131*, 3140–3141.
5. Skorodumova, N. V.; Simak, S. I.; Lundqvist, B. I.; Abrikosov, I. A.; Johansson, B. Quantum Origin of the Oxygen Storage Capability of Ceria. *Phys. Rev. Lett.* **2002**, *89*, 166601.
6. Esch, F.; Fabris, S.; Zhou, L.; Montini, T.; Africh, C.; Fornasiero, P.; Comelli, G.; Rosei, R. Electron Localization Determines Defect Formation on Ceria Substrates. *Science* **2005**, *309*, 752–755.
7. Campbell, C. T.; Peden, C. H. F. Chemistry—Oxygen Vacancies and Catalysis on Ceria Surfaces. *Science* **2005**, *309*, 713–714.
8. Deshpande, S.; Patil, S.; Kuchibhatla, S. V. N. T.; Seal, S. Size Dependency Variation in Lattice Parameter and Valency States in Nanocrystalline Cerium Oxide. *Appl. Phys. Lett.* **2005**, *87*, 133113.
9. Fu, Q.; Saltsburg, H.; Flytzani-Stephanopoulos, M. Active Nonmetallic Au and Pt Species on Ceria-Based Water-Gas Shift Catalysts. *Science* **2003**, *301*, 935–938.
10. Shido, T.; Iwasawa, Y. Regulation of Reaction Intermediate by Reactant in the Water Gas Shift Reaction on CeO_2 in Relation to Reactant-Promoted Mechanism. *J. Catal.* **1992**, *136*, 493–503.
11. Tabakova, T.; Boccuzzi, F.; Manzoli, M.; Sobczak, J. W.; Idakiev, V.; Andreeva, D. A Comparative Study of Nanosized IB/Ceria Catalysts for Low-Temperature Water-Gas Shift Reaction. *Appl. Catal., A* **2006**, *298*, 127–143.
12. Tsunekawa, S.; Sivamohan, R.; Ito, S.; Kasuya, A.; Fukuda, T. Structural Study on Monosize CeO_{2-x} Nanoparticles. *Nanostruct. Mater.* **1999**, *11*, 141–147.
13. Bensalem, A.; Muller, J. C.; Bozonverduraz, F. From Bulk CeO_2 to Supported Cerium Oxygen Clusters—A Diffuse Reflectance Approach. *J. Chem. Soc., Faraday Trans.* **1992**, *88*, 153–154.
14. Tsai, Y. Y.; Oca-Cossio, J.; Agering, K.; Simpson, N. E.; Atkinson, M. A.; Wasserfall, C. H.; Constantinidis, I.; Sigmund, W. Novel Synthesis of Cerium Oxide Nanoparticles for Free Radical Scavenging. *Nanomedicine* **2007**, *2*, 325–332.
15. Deluga, G. A.; Salge, J. R.; Schmidt, L. D.; Verykios, X. E. Renewable Hydrogen from Ethanol by Autothermal Reforming. *Science* **2004**, *303*, 993–997.
16. Mattos, L. V.; Rodino, E.; Resasco, D. E.; Passos, F. B.; Noronha, F. B. Partial Oxidation and CO_2 Reforming of Methane on Pt/Al_2O_3, Pt/ZrO_2, and $Pt/Ce\text{-}ZrO_2$ catalysts. *Fuel Process. Technol.* **2003**, *83*, 147–161.
17. Corma, A.; Atienzar, P.; Garcia, H.; Chane-Ching, J. Y. Hierarchically Mesostructured Doped CeO_2 with Potential for Solar-Cell Use. *Nat. Mater.* **2004**, *3*, 394–397.
18. Kaspar, J.; Fornasiero, P.; Graziani, M. Use of CeO_2-Based Oxides in the Three-Way Catalysis. *Catal. Today* **1999**, *50*, 285–298.
19. Mogensen, M.; Sammes, N. M.; Tompsett, G. A. Physical, Chemical and Electrochemical Properties of Pure and Doped Ceria. *Solid State Ionics* **2000**, *129*, 63–94.
20. Park, S. D.; Vohs, J. M.; Gorte, R. J. Direct Oxidation of Hydrocarbons in a Solid-Oxide Fuel Cell. *Nature* **2000**, *404*, 265–267.
21. Tsunekawa, S.; Fukuda, T.; Kasuya, A. Blue Shift in Ultraviolet Absorption Spectra of Monodisperse CeO_{2-x} Nanoparticles. *J. Appl. Phys.* **2000**, *87*, 1318–1321.
22. Karakoti, A.; Singh, S.; Dowding, J. M.; Seal, S.; Self, W. T. Redox-Active Radical Scavenging Nanomaterials. *Chem. Soc. Rev.* **2010**, *39*, 4422–4432.
23. Chaudhary, Y. S.; Panigrahi, S.; Nayak, S.; Satpati, B.; Bhattacharjee, S.; Kulkarni, N. Facile Synthesis of Ultra-Small Monodisperse Ceria Nanocrystals at Room Temperature and Their Catalytic Activity under Visible Light. *J. Mater. Chem.* **2010**, *20*, 2381–2385.
24. Perez, J. M.; Asati, A.; Nath, S.; Kaittanis, C. Synthesis of Biocompatible Dextran-Coated Nanoceria with PH-Dependent Antioxidant Properties. *Small* **2008**, *4*, 552–556.
25. Heckert, E. G.; Seal, S.; Self, W. T. Fenton-like Reaction Catalyzed by the Rare Earth Inner Transition Metal Cerium. *Environ. Sci. Technol.* **2008**, *42*, 5014–5019.
26. Das, M.; Patil, S.; Bhargava, N.; Kang, J. F.; Riedel, L. M.; Seal, S.; Hickman, J. J. Auto-Catalytic Ceria Nanoparticles Offer Neuroprotection to Adult Rat Spinal Cord Neurons. *Biomaterials* **2007**, *28*, 1918–1925.
27. Imlay, J. A.; Chin, S. M.; Linn, S. Toxic DNA Damage by Hydrogen-Peroxide through the Fenton Reaction *in Vivo* and *in Vitro*. *Science* **1988**, *240*, 640–642.
28. Xue, Y.; Luan, Q. F.; Yang, D.; Yao, X.; Zhou, K. B. Direct Evidence for Hydroxyl Radical Scavenging Activity of Cerium Oxide Nanoparticles. *J. Phys. Chem. C* **2011**, *115*, 4433–4438.
29. Tarnuzzer, R. W.; Colon, J.; Patil, S.; Seal, S. Vacancy Engineered Ceria Nanostructures for Protection from Radiation-Induced Cellular Damage. *Nano Lett.* **2005**, *5*, 2573–2577.
30. Misra, M. K.; Sarwat, M.; Bhakuni, P.; Tuteja, R.; Tuteja, N. Oxidative Stress and Ischemic Myocardial Syndromes. *Med. Sci. Monit.* **2009**, *15*, 209–219.
31. Kumar, B.; Koul, S.; Khandrika, L.; Meacham, R. B.; Koul, H. K. Oxidative Stress is Inherent in Prostate Cancer Cells and is Required for Aggressive Phenotype. *Cancer Res.* **2008**, *68*, 1777–1785.
32. Emerit, J.; Edeas, A.; Bricaire, F. Neurodegenerative Diseases and Oxidative Stress. *Biomed. Pharmacother.* **2004**, *58*, 39–46.
33. Nyska, A.; Kohen, R. Oxidation of Biological Systems: Oxidative Stress Phenomena, Antioxidants, Redox Reactions, and Methods for Their Quantification. *Toxicol. Pathol.* **2002**, *30*, 620–650.
34. Finkel, T.; Holbrook, N. J. Oxidants, Oxidative Stress and the Biology of Ageing. *Nature* **2000**, *408*, 239–247.
35. Niu, J. L.; Azfer, A.; Rogers, L. M.; Wang, X. H.; Kolattukudy, P. E. Cardioprotective Effects of Cerium Oxide Nanoparticles in a Transgenic Murine Model of Cardiomyopathy. *Cardiovasc. Res.* **2007**, *73*, 549–559.
36. Kim, C. K.; Kim, T.; Choi, I.-Y.; Soh, M.; Kim, D.; Kim, Y.-J.; Jang, H.; Yang, H.-S.; Kim, J. Y.; Park, H.-K.; *et al.* Ceria Nanoparticles that can Protect against Ischemic Stroke. *Angew. Chem., Int. Ed.* **2012**, *51*, 11039–11043.
37. Pagliari, F.; Mandoli, C.; Forte, G.; Magnani, E.; Pagliari, S.; Nardone, G.; Licoccia, S.; Minieri, M.; Di Nardo, P.; Traversa, E. Cerium Oxide Nanoparticles Protect Cardiac Progenitor Cells from Oxidative Stress. *ACS Nano* **2012**, *6*, 3767–3775.
38. Colon, J.; Hsieh, N.; Ferguson, A.; Kupelian, P.; Seal, S.; Jenkins, D. W.; Baker, C. H. Cerium Oxide Nanoparticles Protect Gastrointestinal Epithelium from Radiation-Induced Damage by Reduction of Reactive Oxygen Species and Upregulation of Superoxide Dismutase 2. *Nanomedicine* **2010**, *6*, 698–705.
39. Karakoti, A. S.; Singh, S.; Kumar, A.; Malinska, M.; Kuchibhatla, S. V. N. T.; Wozniak, K.; Self, W. T.; Seal, S. PEGylated Nanoceria as Radical Scavenger with Tunable Redox Chemistry. *J. Am. Chem. Soc.* **2009**, *131*, 14144–14145.
40. Ivanov, V. K.; Usatenko, A. V.; Shcherbakov, A. B. Antioxidant Activity of Nanocrystalline Ceria to Anthocyanins. *Russ. J. Inorg. Chem.* **2009**, *54*, 1522–1527.
41. Hirst, S. M.; Karakoti, A. S.; Tyler, R. D.; Sriranganathan, N.; Seal, S.; Reilly, C. M. Anti-Inflammatory Properties of Cerium Oxide Nanoparticles. *Small* **2009**, *5*, 2848–2856.
42. D'Angelo, B.; Santucci, S.; Benedetti, E.; Di Loreto, S.; Phani, R. A.; Falone, S.; Amicarelli, F.; Ceru, M. P.; Cimini, A. Cerium Oxide Nanoparticles Trigger Neuronal Survival in a Human Alzheimer Disease Model By Modulating BDNF Pathway. *Curr. Nanosci.* **2009**, *5*, 167–176.
43. Asati, A.; Santra, S.; Kaittanis, C.; Nath, S.; Perez, J. M. Oxidase-Like Activity of Polymer-Coated Cerium Oxide Nanoparticles. *Angew. Chem., Int. Ed.* **2009**, *48*, 2308–2312.
44. Karakoti, A. S.; Monteiro-Riviere, N. A.; Aggarwal, R.; Davis, J. P.; Narayan, R. J.; Self, W. T.; McGinnis, J.; Seal, S. Nanoceria as Antioxidant: Synthesis and Biomedical Applications. *JOM* **2008**, *60*, 33–37.
45. Singh, N.; Cohen, C. A.; Rzigalinski, B. A. Treatment of Neurodegenerative Disorders with Radical Nanomedicine. *Ann. NY Acad. Sci.* **2007**, *1122*, 219–230.

46. Qi, X. P.; Lewin, A. S.; Sun, L.; Hauswirth, W. W.; Guy, J. Suppression of Mitochondrial Oxidative Stress Provides Long-Term Neuroprotection in Experimental Optic Neuritis. *Invest. Ophthalmol. Visual Sci.* **2007**, *48*, 681–691.
47. Schubert, D.; Dargusch, R.; Raitano, J.; Chan, S. W. Cerium and Yttrium Oxide Nanoparticles are Neuroprotective. *Biochem. Biophys. Res. Commun.* **2006**, *342*, 86–91.
48. Rzigalinski, B. A.; Meehan, K.; Davis, R. M.; Xu, Y.; Miles, W. C.; Cohen, C. A. Radical Nanomedicine. *Nanomedicine* **2006**, *1*, 399–412.
49. Chen, J. P.; Patil, S.; Seal, S.; McGinnis, J. F. Rare Earth Nanoparticles Prevent Retinal Degeneration Induced by Intracellular Peroxides. *Nat. Nanotechnol.* **2006**, *1*, 142–150.
50. Asati, A.; Santra, S.; Kaittanis, C.; Perez, J. M. Surface-Charge-Dependent Cell Localization and Cytotoxicity of Cerium Oxide Nanoparticles. *ACS Nano* **2010**, *4*, 5321–5331.
51. Cao, G. H.; Alessio, H. M.; Cutler, R. G. Oxygen-Radical Absorbency Capacity Assay for Antioxidants. *Free Radical Biol. Med.* **1993**, *14*, 303–311.
52. Lucente-Schultz, R. M.; Moore, V. C.; Leonard, A. D.; Price, B. K.; Kosynkin, D. V.; Lu, M.; Partha, R.; Conyers, J. L.; Tour, J. M. Antioxidant Single-Walled Carbon Nanotubes. *J. Am. Chem. Soc.* **2009**, *131*, 3934–3941.
53. Qin, Y.; Lu, M.; Gong, X. G. Dihydrorhodamine 123 is Superior to 2,7-Dichlorodihydrofluorescein Diacetate and Dihydrorhodamine 6G in Detecting Intracellular Hydrogen Peroxide in Tumor Cells. *Cell Biol. Int.* **2008**, *32*, 224–228.
54. Carlson, C.; Hussain, S. M.; Schrand, A. M.; Braydich-Stolle, L. K.; Hess, K. L.; Jones, R. L.; Schlager, J. J. Unique Cellular Interaction of Silver Nanoparticles: Size-Dependent Generation of Reactive Oxygen Species. *J. Phys. Chem. B* **2008**, *112*, 13608–13619.
55. Lee, S. S.; Zhu, H. G.; Contreras, E. Q.; Prakash, A.; Puppala, H. L.; Colvin, V. L. High Temperature Decomposition of Cerium Precursors to Form Ceria Nanocrystal Libraries for Biological Applications. *Chem. Mater.* **2012**, *24*, 424–432.
56. Prakash, A.; Zhu, H. G.; Jones, C. J.; Benoit, D. N.; Ellsworth, A. Z.; Bryant, E. L.; Colvin, V. L. Bilayers as Phase Transfer Agents for Nanocrystals Prepared in Nonpolar Solvents. *ACS Nano* **2009**, *3*, 2139–2146.
57. Duan, H. W.; Kuang, M.; Wang, X. X.; Wang, Y. A.; Mao, H.; Nie, S. M. Reexamining the Effects of Particle Size and Surface Chemistry on the Magnetic Properties of Iron Oxide Nanocrystals: New Insights into Spin Disorder and Proton Relaxivity. *J. Phys. Chem. C* **2008**, *112*, 8127–8131.
58. Yu, W. W.; Chang, E.; Falkner, J. C.; Zhang, J. Y.; Al-Somali, A. M.; Sayes, C. M.; Johns, J.; Drezek, R.; Colvin, V. L. Forming Biocompatible and Nonaggregated Nanocrystals in Water Using Amphiphilic Polymers. *J. Am. Chem. Soc.* **2007**, *129*, 2871–2879.
59. Djuricic, B.; Pickering, S. Nanostructured Cerium Oxide: Preparation and Properties of Weakly-Agglomerated Powders. *J. Eur. Ceram. Soc.* **1999**, *19*, 1925–1934.
60. Scholes, F. H.; Hughes, A. E.; Hardin, S. G.; Lynch, P.; Miller, P. R. Influence of Hhydrogen Peroxide in the Preparation of Nanocrystalline Ceria. *Chem. Mater.* **2007**, *19*, 2321–2328.
61. Korsvik, C.; Patil, S.; Seal, S.; Self, W. T. Superoxide Dismutase Mimetic Properties Exhibited by Vacancy Engineered Ceria Nanoparticles. *Chem. Commun.* **2007**, 1056–1058.
62. Gogate, P. R.; Pandit, A. B. A Review of Imperative Technologies for Wastewater Treatment I: Oxidation Technologies at Ambient Conditions. *Adv. Environ. Res.* **2004**, *8*, 501–551.
63. Chen, R. Z.; Pignatello, J. J. Role of Quinone Intermediates as Electron Shuttles in Fenton and Photoassisted Fenton Oxidations of Aromatic Compounds. *Environ. Sci. Technol.* **1997**, *31*, 2399–2406.
64. Pirmohamed, T.; Dowding, J. M.; Singh, S.; Wasserman, B.; Heckert, E.; Karakoti, A. S.; King, J. E. S.; Seal, S.; Self, W. T. Nanoceria Exhibit Redox State-Dependent Catalase Mimetic Activity. *Chem. Commun.* **2010**, *46*, 2736–2738.
65. Yildiz, G.; Demiryurek, A. T.; Sahin-Erdemli, I.; Kanzik, I. Comparison of Antioxidant Activities of Aminoguanidine, Methylguanidine and Guanidine by Luminol-Enhanced Chemiluminescence. *Br. J. Pharmacol.* **1998**, *124*, 905–910.
66. King, D. W.; Lounsbury, H. A.; Millero, F. J. Rates and Mechanism of Fe(II) Oxidation at Nanomolar Total Iron Concentrations. *Environ. Sci. Technol.* **1995**, *29*, 818–824.
67. Wu, L. M.; Shen, X. M.; Liu, D. Q. A Novel GC-MS Method for Rapid Determination of Headspace Oxygen in Vials of Pharmaceutical Formulations. *J. Pharm. Biomed. Anal.* **2008**, *48*, 8–12.
68. Qiu, L. M.; Liu, F.; Zhao, L. Z.; Ma, Y.; Yao, J. N. Comparative XPS Study of Surface Reduction for Nanocrystalline and Microcrystalline Ceria Powder. *Appl. Surf. Sci.* **2006**, *252*, 4931–4935.
69. Lucio, M.; Nunes, C.; Gaspar, D.; Ferreira, H.; Lima, J. L. F. C.; Reis, S. Antioxidant Activity of Vitamin E and Trolox: Understanding of the Factors that Govern Lipid Peroxidation Studies *in Vitro*. *Food Biophys.* **2009**, *4*, 312–320.
70. Hoyt, K. R.; Gallagher, A. J.; Hastings, T. G.; Reynolds, I. J. Characterization of Hydrogen Peroxide Toxicity in Cultured Rat Forebrain Neurons. *Neurochem. Res.* **1997**, *22*, 333–340.
71. Turnwald, S. E.; Lorier, M. A.; Wright, L. J.; Mucalo, M. R. Oleic Acid Oxidation Using Hydrogen Peroxide in Conjunction with Transition Metal Catalysis. *J. Mater. Sci. Lett.* **1998**, *17*, 1305–1307.
72. Swern, D.; Billen, G. N.; Findley, T. W.; Scanlan, J. T. Hydroxylation of Monounsaturated Fatty Materials with Hydrogen Peroxide. *J. Am. Chem. Soc.* **1945**, *67*, 1786–1789.
73. Noureddini, H.; Kanabur, M. Liquid-Phase Catalytic Oxidation of Unsaturated Fatty Acids. *J. Am. Oil Chem. Soc.* **1999**, *76*, 305–312.
74. Smith, A. M.; Nie, S. Minimizing the Hydrodynamic Size of Quantum Dots with Multifunctional Multidentate Polymer Ligands. *J. Am. Chem. Soc.* **2008**, *130*, 11278–11279.
75. Zhang, X. M.; Neiner, D.; Wang, S. Z.; Louie, A. Y.; Kauzlarich, S. M. A New Solution Route to Hydrogen-Terminated Silicon Nanoparticles: Synthesis, Functionalization and Water Stability. *Nanotechnology* **2007**, *18*, 95601.
76. Wang, K. T.; Iliopoulos, I.; Audebert, R. Viscometric Behavior of Hydrophobically Modified Poly(sodium acrylate). *Polym. Bull.* **1988**, *20*, 577–582.
77. Kilpatrick, K.; Novoa, J. A.; Hancock, T.; Guerriero, C. J.; Wipf, P.; Brodsky, J. L.; Segatori, L. Chemical Induction of Hsp70 Reduces α-Synuclein Aggregation in Neuroglioma Cells. *ACS Chem. Biol.* **2013**, *8*, 1460–1468.